RSC Advances

PAPER

View Article Online
View Journal | View Issue

Cite this: *RSC Adv.*, 2017, **7**, 11862

The effect of cobalt promoter on the CO methanation reaction over MoS_2 catalyst: a density functional study†

Chunyun Zhang,[a] Bonan Liu,[b] Yuxian Wang,[a] Liang Zhao,*[a] Jin Zhang,[b] Qiuyun Zong,*[b] Jinsen Gao[a] and Chunming Xu[a]

The potential mechanism of sulfur-resistant CO methanation was theoretically investigated *via* density functional theory (DFT + D) calculations. Comparisons were made between modified Co–MoS_2 and pure MoS_2 catalysts and we highlighted the distinguished CO methanation pathway in the presence of Co-promoter. Multiple intermediates were formed at different catalytic sites during the reaction, which further increased the mechanism complexity. The results obtained from Co–MoS_2 imply that the CH_3OH species could be formed along the most feasible reaction pathway on Mo catalyst termination; the subsequent dissociation of CH_3OH into CH_3 and OH was found to be the rate determining step with a reaction barrier of 29.35 kcal mol^{-1} at 750 K. On the S edge of Co–MoS_2, the CH_2OH intermediate could be formed as a result of CH_2O reacting with adsorbed hydrogen, and subsequent CH_2OH dissociation was noted to release CH_2. Afterwards, consecutive hydrogenation of CH_2 led to the final CH_4 yield. On S catalyst termination, it was suggested that the CHO intermediate formation played a key role as the rate-determining step with the reaction barrier of 19.56 kcal mol^{-1} at 750 K. By comparing the CO methanation energy profiles over different samples, it was discovered that the Co-promoter did possess promoting effects at both the Mo edge and the S edge of the catalyst; note that this enhancement at the Mo edge was superior to that at the S edge, especially for larger scale applications. Moreover, after doping with Co, the OH species was easier to remove in terms of H_2O molecules, which created enough vacant active sites for a continuous reaction.

Received 28th November 2016
Accepted 2nd February 2017

DOI: 10.1039/c6ra27422f

rsc.li/rsc-advances

1. Introduction

As is well-known, natural gas is an important clean fuel that is environmentally friendly and convenient to transport. Its main component is CH_4, which has high calorific value and is a comparably safe and efficient energy carrier. On the other hand, modern chemistry requires coal cleaning combustion and upgrade for sustainable development, especially in those coal rich countries such as China. As an effective method, methanation of carbon monoxide ($CO + 3H_2 \rightarrow CH_4 + H_2O$, $\Delta = -206.2$ kJ mol^{-1}), from syngas generated by coal (CO and H_2 are major contents), to produce synthesized natural gas 'SNG' (CH_4) has attracted significant attention, particularly for its low pollutant emissions.[1–3]

Numerous metals, such as rhodium, ruthenium, cobalt and nickel, have been studied as catalysts for the industrial CO methanation process, and different kinds of metals are found to have different advantages. For example, rhodium and ruthenium have relatively higher activities, whereas nickel relies on a much lower cost.[4–6] Nickel-based catalysts were once routinely used in industry, but they are very sensitive to sulfur compounds and thus there is a very rigorous restriction on upstream syngas sulfur containing levels;[7,8] the relevant syngas desulfurization remarkably increases the production cost. Unlike conventional products, molybdenum-based catalysts have shown excellent CO methanation performance with desired sulfur-resistance, therefore enabling a so called 'sulfur-resistant CO methanation reaction'.[9–16] Rather than 'poisoning the metal catalytic sites', the introduction of sulfur plays a positive and essential role in Mo-based catalyst activation; the pre-sulfurized active sites (MoS_2) are responsible for effective CO conversion.[17] In further research attempts, a second metal was added to promote the stability and activity of MoS_2 catalysts. Among various metal-promoters, Co exhibits a superior promoting effect on the activity of Mo/Al catalysts, which have been the most successful catalysts for sulfur-resistant CO methanation.[18,19] Besides, cobalt also enhances the stability of

[a]State Key Laboratory of Heavy Oil Processing, China University of Petroleum (Beijing), 18 Fuxue Road, Beijing, 102249, China. E-mail: liangzhao@cup.edu.cn; Tel: +86-10-89739078

[b]Qingdao LianXin Catalytic Materials Co. Ltd, Qingdao, 266300, China. E-mail: zqy1959@163.com; Tel: +86-532-82279823

† Electronic supplementary information (ESI) available. See DOI: 10.1039/c6ra27422f

Mo-based catalysts within CO methanation, especially under a water-containing atmosphere, where cobalt addition not only provides extra active sites, but also protects the active MoS_2 phase.[20]

Numerous efforts have been made to study CO methanation mechanisms on different kinds of Ni-based catalysts;[21–25] however, research on methanation mechanisms employing MoS_2-based catalysts are uncommonly seen. Although a series of intermediates do exist during the reaction, which may increase the complexity of the mechanism study, methane has been proved to be the main product for CO methanation over MoS_2 catalysts, as supported by both theoretical and experimental observations.[26,27] Unlike the reaction on the pure Mo metal surface, adsorbed CO on the MoS_2 surface is unlikely to dissociate into C and O atoms before hydrogenation.[26] Shi *et al.* illustrated the optimal pathway for CO methanation over pure MoS_2 catalysts, in which intermediate CH_2OH was formed, and finally, CH_4 was obtained by consecutive CH_2 hydrogenation.[28] DFT calculations have reported that doping K onto the MoS_2 surface managed to enhance the CO adsorption efficiency by changing the local electronic environment, and reducing the barrier to C–C species formation; however the complete CO methanation route has still not been discussed.[29] To the best of our knowledge, there has been no research focusing on the complete CO methanation mechanism on cobalt doped MoS_2 catalysts. Therefore, an investigation on the degree of promotion of cobalt for the CO methanation reaction over molybdenum-based catalysts is urgently needed to gain profound insight into CO methanation mechanisms on Co–MoS_2.

Our work addresses the study of the fundamental mechanism of Co–MoS_2 promoted CO methanation (sulfur-resistant) by the DFT + D (dispersion force correction) method. We firstly investigated the adsorption performance of reactants, intermediates and products. Afterwards, all possible reaction pathways were designed and compared to identify the most favorable route of CO methanation at different surfaces of Co–MoS_2. Energy profiles in optimal paths at 750 K were investigated on both edges of pure MoS_2 and Co–MoS_2 catalysts. Advances were also achieved by comparing the sulfur-resistant methanation performance over MoS_2 catalysts and Co–MoS_2 catalysts.

2. Computational details

Calculations based on density functional theory (DFT) were performed with the Dmol^3 program in the Material Studio Package.[30–32] The generalized gradient approach (GGA)[33] and exchange–correlation potential developed by Perdew, Burke, and Ernzerhof (PBE),[34] with the Grimme method[35] for dispersion corrections (DFT-D correction) were adopted. Double numerical basis sets plus polarization functions (DNP) were used to represent atomic orbitals, and DFT semi-core pseudopotentials (DSPPs) were employed for metal core treatment. The orbital cutoff was 4.9 Å and the Monkhorst–Pack mesh *k*-point $f(2 \times 2 \times 1)$ was adopted. The SCF convergence criterion was 1.0×10^{-6} Ha per atom, and smearing was set as 2.0×10^{-3} Ha to accelerate the convergence of orbital occupation. Convergence tolerances of energy, maximum force, and maximum displacement were set as 1.0×10^{-5} Ha, 2.0×10^{-3} Ha Å^{-1}, and 5.0×10^{-3} Å, respectively. Transition state (TS) searches were carried out at the same accuracy by complete linear synchronous transit (LST)/quadratic synchronous transit (QST) methods.[36] The method starts by LST pathway connection of the reactant and product, after which the TS approximation was used to perform QST maximization. Afterwards, another conjugated gradient minimization was performed, based on the maximization point and the cycle repeats until the calculation was converged. Maximum iteration steps were 1000 and DIIS was used to accelerate the convergence of orbitals. Spin polarization was applied in the calculation process on account of the magnetic properties of Co. The transition states in this work have been proved by imaginary frequency.

The MoS_2 (10–10) surface was represented as four S–Mo–S slabs with the bottom two layers constrained to crystal lattice positions.[37–44] The Mo edge and the S edge of pure MoS_2 catalysts were reported to exist in realistic conditions, and both edges achieved stable equilibrium structures by sulfur reconstruction.[45–49] Along with sulfur reconstruction, the S vacancies created active sites. Co–MoS_2 was represented by 25% Co substitution of Mo on the surface.[50] Herein, we define 100% sulfur coverage as corresponding to two sulfurs for each Mo atom on the surface. It is quite controversial to discuss which edge is more favorable for the location of Co-promoter; some studies revealed that the S edge was better,[47,49] with 50% sulfur coverage, while some articles supported the Mo edge.[51] Besides, many more models of Co–MoS_2 catalysts with various Co content, including Mo edge and S edge, have been discussed.[52–54] The Mo termination of 25% substituted Co–MoS_2 with 25% sulfur coverage, and the S termination with 50% sulfur coverage were considered to be thermodynamically stable in industrial reactions,[50,55] as shown in Fig. 1(a) and (b). Vacuum thickness of 15 Å was set in each model to avoid electronic coupling between adjacent slabs. For simplicity, the Mo termination of Co–MoS_2, and the S termination of Co–MoS_2 were recorded as T_1 and T_2, respectively. After geometry optimization based on the parameters mentioned above, surface Co was observed to relax inward by 0.467 Å on the Mo termination and 0.187 Å on the S termination, both of which were in good accordance with the values reported previously (0.46 Å and 0.17 Å, respectively).[50]

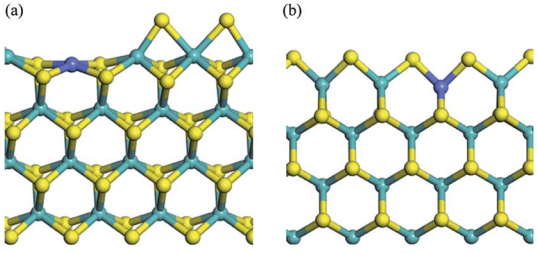

Fig. 1 Crystal structures of T_1 (a) and T_2 (b) terminations. Mo/S/Co centers are shown as blue balls, yellow balls, and purple balls, respectively.

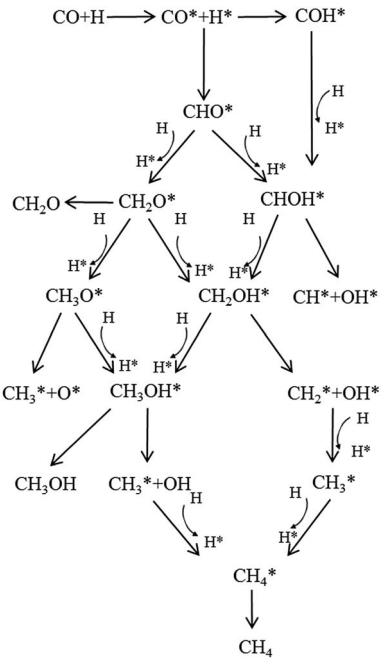

Fig. 2 Possible pathways for the CO methanation reaction.

The adsorption energy (E_{ads}) was calculated from the energy difference between the adsorption state and free states, as shown in eqn (1). Herein, $E_{(ads+slab)}$ is the energy of the surface containing the adsorbate, $E_{(slab)}$ is the energy of the clean surface, and $E_{(ads)}$ is the energy of the adsorbing molecule in the gas state. Negative E_{ads} value indicates an exothermic adsorption, and thus the most negative adsorption energy signifies the most stable adsorption configuration. The active energy barrier (E_a) is calculated according to eqn (2), and reaction energy (E_{sep}) is calculated by eqn (3).

$$E_{ads} = E_{(ads+slab)} - E_{(ads)} - E_{(slab)} \quad (1)$$

$$E_a = E_{TS} - E_R \quad (2)$$

$$E_{sep} = E_P - E_R \quad (3)$$

Herein, E_{TS} means the energy of the transition state (TS) system, and E_R, E_P mean the energy of the reactant system and product system, respectively. Taking into account all possible pathways *via* different intermediates, we proposed a detailed CO methanation reaction network, which is schematically illustrated in Fig. 2. All the pathways shown in Fig. 2 were investigated in this study to find the optimal path for the CO methanation reaction over Co–MoS_2 catalysts.

3. Results and discussions

3.1. Adsorption of reactants, intermediates and products

The adsorption performance of all species involved in the CO methanation on T_1 and T_2 terminations has been considered. Here, we focus on CO, H, CH_2O, and CH_3OH intermediates; the other intermediates like CHO, COH, CH_3O, H_2O and so on are summarized in the ESI.† Adsorption energies E_{ads} and adsorption geometry parameters are listed in Table 1. Fig. 3 illustrates the adsorption configurations of intermediates involved in the most stable states on T_1 and T_2, where although many more adsorption sites and configurations have been considered, only two stable adsorption configurations with the largest E_{ads} are described in this paper.

H atoms on T_1 termination preferred to adsorb on top of the bare Co site (−55.58 kcal mol^{-1}, −53.50 kcal mol^{-1} (ref. 50)) and bare Mo site (−53.04 kcal mol^{-1}, −50.50 kcal mol^{-1} (ref. 50)) than the S site (−44.51 kcal mol^{-1}, −44.05 kcal mol^{-1} (ref. 50)), which revealed that the Co-promoter enhanced the adsorption performance of H atoms by creating new adsorption sites. Herein, adsorption energy values of the H adatom, obtained from literature,[51] are listed as reference values, which were determined with VASP using the PAW method, PW91. On T_2 termination, however, the interactions between H atoms and catalysts were relaxed by Co-promoter, since the H atom has stronger interactions with the bridge Mo–Mo site (−59.27 kcal mol^{-1}, −57.65 kcal mol^{-1} (ref. 50)) than the bridge Co–Mo site (−52.35 kcal mol^{-1}) or S site (−50.50 kcal mol^{-1}). For O and OH groups, as described in ESI,† the Co site did not show conspicuous advantages over the Mo site on both terminations, which was due to the electronegativity of the O atom. CO was observed to be stabilized on the top of the bare Co site or Mo site with its carbon atom for both T_1 and T_2 terminations. For T_1, the Co site (−45.43 kcal mol^{-1}) was more active than the Mo site (−26.98 kcal mol^{-1}). For T_2, however, CO adsorbing at the Co site (−24.91 kcal mol^{-1}) or Mo site (−24.67 kcal mol^{-1}) resulted in similar adsorption energies. Structurally, the calculated Co–C

Table 1 Adsorption energies (E_{ads}, in kcal mol^{-1}) and the geometry parameters (in Å) of key intermediates on T_1 and T_2 terminations

	T_1		T_2	
	E_{ads}	$d_{C-O/Co-C/Co-O/Co-H/Mo-C/Mo-O/Mo-H}$	E_{ads}	$d_{C-O/Co-C/Co-O/Co^{-}H/Mo^{-}C/Mo^{-}O/Mo^{-}H}$
CO (a)	−45.43	1.15/1.77/—/—/—/—/—	−24.91	1.16/1.78/—/—/—/—/—
CO (b)	−26.98	1.16/—/—/—/2.06/—/—	−24.67	1.16/—/—/—/2.05/—/—
H (a)	−55.58	—/—/—/1.48/—/—/—	−59.27	—/—/—/—/—/—/1.93, 1.81
H (b)	−53.04	—/—/—/—/—/—/1.71	−52.35	—/—/—/1.78/—/—/1.77
CH_2O (a)	−30.87	1.38/2.02/—/—/—/1.98/—	−12.62	1.34/—/—/—/2.21/2.03/—
CH_2O (b)	−20.37	1.29/—/1.92/—/2.46/—/—	−11.47	1.23/—/—/—/—/2.39/—
CH_3OH (a)	−27.99	1.46/—/2.04/—/—/—/—	−13.20	1.45/—/—/—/—/2.45/—
CH_3OH (b)	−22.28	1.45/2.57/—/—/—/2.31/—	−12.15	1.46/—/2.22/—/—/2.58/—

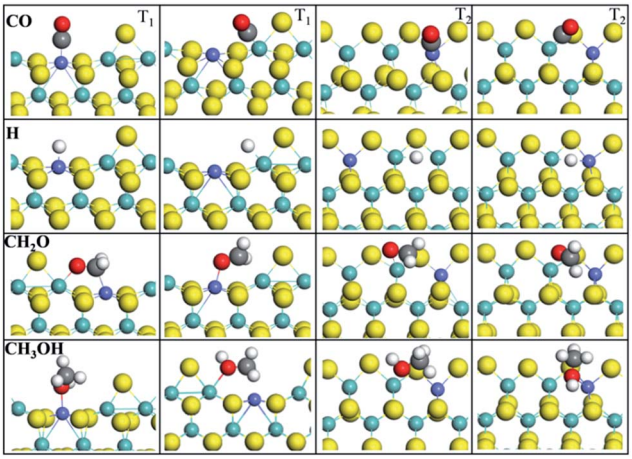

Fig. 3 Adsorption configurations of CO, H, CH_2O, and CH_3OH in stable states on T_1 and T_2 terminations.

distances were 1.77 Å for T_1 termination and 1.78 Å for T_2, and the obtained Mo–C distances were 2.06 Å for T_1 and 2.05 Å for T_2. Besides, in spite of distinct energy differences, the four adsorption structures have equal C–O distances, which were all activated into about 1.16 Å. CH_2O on T_1 was prone to adsorbing at the Co–Mo bridge site, while on T_2 it was inclined to interact with the Mo site *via* the O atom. For CH_3OH, it was found that except for the Co–Mo bridge site, which is a priority on both T_1 and T_2, the Co site on T_1 and Mo site on T_2 take precedence as well. It was concluded that most C1 intermediates prefer to adsorb at the Co site or adjoining Mo–Co site, as shown in ESI,† and it revealed that the Co-promoter provided more active sites by transforming the structure and altering the electronic distribution of MoS_2, which made it easier for C1 species or H atoms to be adsorbed.

For a better understanding of the effect of cobalt-promoter on the electron distribution of MoS_2, population analysis was calculated to study electron transfer. It was found that when compared with the Mo site, the Co atom obtained more electrons transferred from the carbon atom in the C1 species, which made the binding interaction between carbon and cobalt stronger. Taking the CO molecule as an example, in the adsorption configurations of CO, charge separations were found as follows: $Mo^{-0.141}$–$C^{0.309}$–$O^{-0.118}$ on the Mo edge of MoS_2, $Co^{-0.469}$–$C^{0.508}$–$O^{-0.128}$ on the Mo edge of Co–MoS_2, $Mo^{-0.085}$–$C^{0.325}$–$O^{-0.162}$ on the S edge of MoS_2, and $Mo^{-0.468}$–$C^{0.471}$–O^{-134} on the S edge of Co–MoS_2. This explains why Co or Co–Mo active sites were more favorable than the Mo site for the adsorption of most C1 species and why carbon was inclined to interact with the cobalt atom, while the Mo site was more favorable than the Co site for oxygen atoms. Moreover, strong interactions between molecule and catalyst could weaken some bonds inside the adsorbate, which would decrease the difficulty of bond breaking in the adsorbate, or attack by other atoms.

3.2. Overview of the CO methanation pathway on Co–MoS_2

Calculated reaction barriers and reaction energies of all possible elementary steps for CO methanation on T_1 and T_2 termination are separately depicted in Fig. 4 and 5. Configurations of reactants, transition states, and products involved, with detailed information including bond lengths and angles are summarized in the ESI.†

3.2.1. CO methanation on T_1 termination. CO methanation starts from the incorporation of adsorbed CO and a nearby hydrogen atom; COH and CHO are two possible products for the first elementary step. Since the formation of CHO is more kinetically favorable than COH (E_a = 25.08 kcal mol^{-1} *vs.* 63.07 kcal mol^{-1}), CHO is supposed to be the first intermediate from CO reacting with the hydrogen adatom (Fig. 4). The hydrogenation of COH was not successfully investigated in this study because the reaction barrier of the formation of COH was higher than the reaction barrier of the rate determining step along the most favorable reaction pathway, which would be determined later.

After the formation of CHO, CHOH (+27.21 kcal mol^{-1}) and CH_2O (+12.77 kcal mol^{-1}) were then obtained by CHO reacting with adjacent hydrogen adatoms. In this step, the favorable product depended on which atom, oxygen or carbon in the CHO, was easier to attack by the independently co-adsorbed hydrogen. Apparently, CH_2O was favored over the CHOH intermediate. Based on our calculations, neither the dissociation of CHOH into CH + OH (+43.73 kcal mol^{-1}) nor the decomposition of CH_2O into CH_2 and O (+43.99 kcal mol^{-1}) occur easily. Similarly, the formation of the CH_3O intermediate through CH_2O was not available on account of the high reaction barrier (+38.45 kcal mol^{-1}). Interestingly, although CH_2OH can be produced by either CHOH or CH_2O reacting with adjacent hydrogen adatoms, the CH_2O route (+20.50 kcal mol^{-1}) was easier than the CHOH route (+28.65 kcal mol^{-1}); therefore, the preceding step is the further hydrogenation of CHO to form CH_2O, followed by CH_2O hydrogenated into CH_2OH.

With regard to the subsequent reaction of CH_2OH, further hydrogenation of CH_2OH into CH_3OH was far more advantageous than the decomposition of CH_2OH into CH_2 and OH (E_a = 10.11 *vs.* 31.62 kcal mol^{-1}). Moreover, the reaction barrier of CH_3OH dissociation into CH_3 and OH (+27.15 kcal mol^{-1}) was likewise lower than CH_2OH dissociation; therefore, CH_3OH and CH_3 are both favorable intermediates in the optimal pathway. Moreover, since the dissociation energy of CH_3OH (+27.15 kcal mol^{-1}) is close to the CH_3OH desorption energy of 27.99 kcal mol^{-1}, there is the possibility of the release of free CH_3OH; this accounts for the fact that CH_3OH is a side gas product, which agrees well with literature.[56–58] Eventually, the final product, CH_4, was attained by CH_3 reacting with adsorbed hydrogen with the reaction barrier of 12.96 kcal mol^{-1}.

Based on our calculations, the most feasible pathway for CO methanation on T_1 termination is CO + 5H → CHO + 4H → CH_2O + 3H → CH_2OH + 2H → CH_3OH + H → CH_3 + OH + H → CH_4 + OH, as illustrated in Fig. 4, in which the dissociation of CH_3OH into CH_3 and OH is the rate-determining step.

3.2.2. CO methanation on T_2 termination. From Fig. 5, two possible routes exist for the first reaction step of CO hydrogenation on T_2 termination, in which either CHO or COH is generated. The formation of CHO is more kinetically favorable than COH (E_a = 16.99 *vs.* 64.43 kcal mol^{-1}). Although the reaction barrier of the CHO subsequent reaction with hydrogen

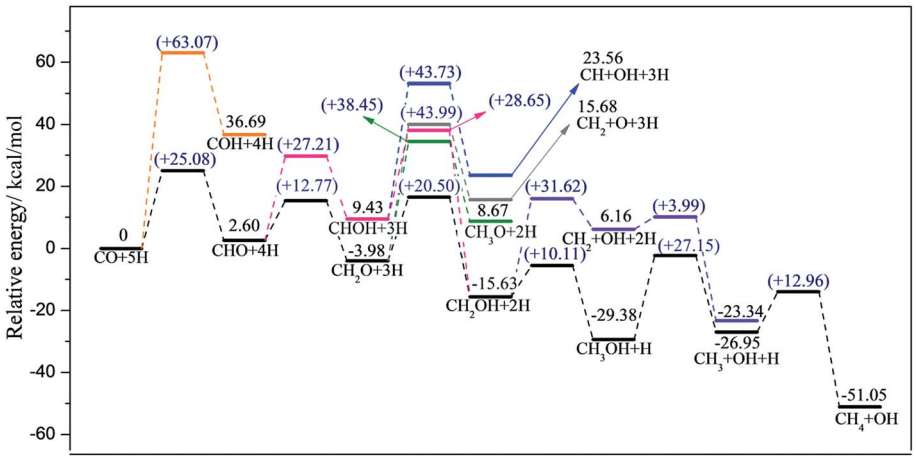

Fig. 4 Energy profiles along different pathways of CO methanation on T_1 termination, where the black line represents the most favorable pathway. Zero energy corresponds to the co-adsorption of CO and H atoms on T_1 termination.

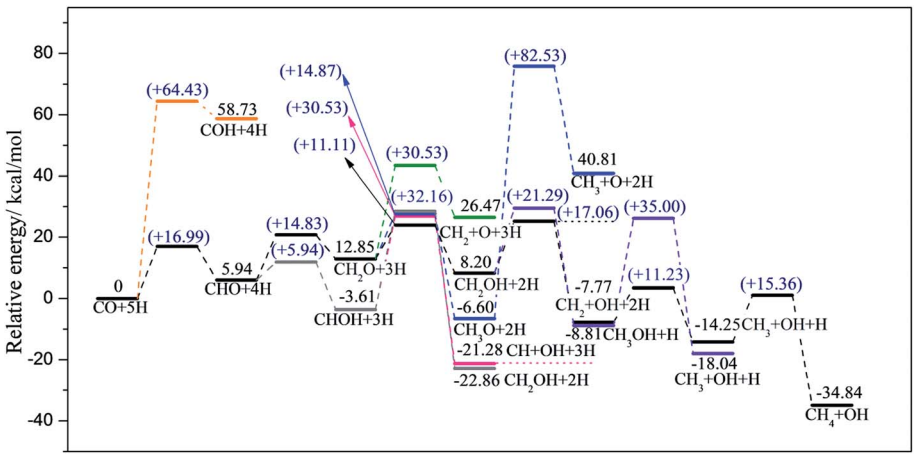

Fig. 5 Energy profiles along different pathways of CO methanation on T_2 termination, where the black line represents the most favorable pathway. Zero energy corresponds to the co-adsorption of CO and H atoms on T_2 termination.

to form CHOH is lower than the formation of CH_2O (E_a = 5.94 *vs.* 14.83 kcal mol^{-1}), the next steps to form CH_2OH by CHOH hydrogenation (+32.16 kcal mol^{-1}), or dissociation into CH and OH (+30.53 kcal mol^{-1}) are both difficult. In contrast, the formation of CH_2OH (+11.11 kcal mol^{-1}) or CH_3O (+14.87 kcal mol^{-1}) *via* CH_2O reacting with nearby H adatoms is easier. Therefore, the result is the same as with T_1 termination, in which CHO was the first intermediate by CO reacting with adsorbed hydrogen, and hence the second intermediate was CH_2O. Besides, desorption of CH_2O (+12.62 kcal mol^{-1}) was able to occur, therefore formaldehyde, CH_2O, must exist in the gas products. Nonetheless, the dissociation of CH_2O into CH_2 and O adatom ensued with difficulty. In addition, CH_3 species were hard to obtain by CH_3O dissociation with the reaction barrier up to 82.53 kcal mol^{-1}. Accordingly, CH_2OH was the next favored intermediate along the optimal CO methanation pathway on T_2 termination.

Regarding the next reaction of adsorbed CH_2OH, two routes were possible, one of which generated CH_3OH *via* the bonding of the carbon atom in CH_2OH with the nearby adsorbed hydrogen, and the other one produced CH_2 and OH. As can be seen from Fig. 5, both steps are kinetically favorable (E_a = 21.29 *vs.* 17.06 kcal mol^{-1}). However, the dissociation of CH_3OH into CH_3 and OH was difficult, with the barrier of 35.00 kcal mol^{-1} being much higher than its desorption energy 13.20 kcal mol^{-1}, which means that CH_3OH was more likely to desorb rather than react further. Therefore, the next intermediate along the optimal path was CH_2, while CH_3OH was a favorable species in the final gas products. Subsequently, CH_3 was obtained *via* CH_2 interaction with a nearby H adatom (E_a = 11.23 kcal mol^{-1}). Furthermore, the barrier of further conversion of CH_3 into the final product CH_4 was 15.36 kcal mol^{-1}.

Based on the discussions above, the most favorable pathway for CO methanation on T_2 termination was clear, which was CO + 5H → CHO + 4H → CH_2O + 3H → CH_2OH + 2H → CH_2 + OH + H → CH_3 + OH + H → CH_4 + OH, and the dissociation of CH_2OH into CH_2 and OH groups was the rate-determining step at 0 K.

3.3. Comparison of the CO methanation mechanism of pure MoS_2 and Co–MoS_2

For simplicity, the Mo and S terminations of pure MoS_2 catalysts were named T_3 and T_4, respectively. As reported earlier, the CO methanation reaction route over pure MoS_2 catalyst (both T_3 and T_4) is CO + 5H → CHO + 4H → CH_2O + 3H → CH_2OH + 2H → CH_2 + OH + H → CH_3 + OH + H → CH_4 + OH.[28] Reaction barriers and energies of the CO methanation reaction on T_3 and T_4 terminations were recalculated by the DFT + D method with the computational accuracy as mentioned above in this paper. Recalculated reaction energies and previously announced energy values along the most favorable pathway on T_3 and T_4 terminations are summarized in Table 2, in which E_{sep} and E_a are defined as reaction energies and reaction barriers, respectively. As can be seen, part of the calculated energies were a bit different from previously reported values,[28] since we considered dispersion force correction and we consider more adsorption configurations based on literature.[28] Configurations of reactants, transition states, and products on both T_3 and T_4 edges, with detailed information including bond lengths and angles are summarized in the ESI.†

Considering realistic temperature conditions for industrial CO methanation, free energy changes of all reactants, intermediates, and products at 750 K were calculated, and energy profiles along the optimal paths on four edges at 750 K were calculated and are depicted in Fig. 6 and 7. Fig. 6 summarizes the most feasible CO methanation reaction routines on T_1 and T_3, and Fig. 7 depicts the most favorable pathways on T_2 and T_4 terminations; in both figures, all the configurations of reactants, transition states and products involved in the optimal pathways are given. The configurations of species involved in other feasible routes on T_1 and T_2 terminations are given in the ESI.† As seen in Fig. 6, except for the last two steps, it was found that the reaction barriers on T_1 termination were smaller than on T_3 termination, in general. The rate determining step on T_3 was the only endothermic elementary step, CO + H → CHO, the reaction barrier of which was up to 40.41 kcal mol^{-1}. However, after doping Co-promoter into MoS_2, the reaction barrier of CO hydrogenation into CHO was decreased to 20.64 kcal mol^{-1}. For T_1 termination, as mentioned above, CH_3OH was a favorable intermediate with low formation barrier and cleavage of the C–O bond of CH_3OH was the rate determining step for CO methanation on T_1 termination with the reaction barrier of 29.35 kcal mol^{-1}. Obviously, the Co-promoter lowered the reaction barrier by about 11 kcal mol^{-1} and thus, accelerated the reaction kinetically on Mo termination.

For S termination (Fig. 7), it was found that the reaction barriers on T_2 termination were obviously smaller than the reaction barriers on T_4 terminations, except for the third step. The formation of CHO (E_a = 19.56 kcal mol^{-1}) was the rate determining step for T_2, while for T_4, not only the formation of CHO (E_a = 21.46 kcal mol^{-1}), but also the formation of CH_2O (E_a = 20.05 kcal mol^{-1}), the dissociation of CH_2OH (E_a = 20.03 kcal mol^{-1}) and the formation of CH_4 (E_a = 21.29 kcal mol^{-1}) had higher reaction barriers. It can be likewise deduced that the CO methanation reaction occurred with kinetically less effort on T_2 than on T_4 termination, and Co lowered the reaction barriers of the rate-determining step by 2 kcal mol^{-1} on S termination.

On the basis of comparison, the Co-promoter plays a promoting role in the CO methanation reaction both on S and Mo terminations to different degrees, which is in good agreement with experimental studies.[59–63] Except for the last step, CH_3 + H → CH_4, which occurred more easily on T_3 termination than on T_4 termination, S termination showed the superiority of the other CO methanation steps to Mo termination over pure MoS_2 catalysts. However, from Fig. 6 and 7, it is apparent that S termination did not precede Mo termination over Co–MoS_2 catalysts as significantly as over unsupported MoS_2 catalysts for the CO methanation reaction, since the overall reaction barriers on S termination were closer to the Mo edge after doping Co-promoter.

3.4. Formation of H_2O

Formation of H_2O *via* OH reacting with a H adatom on four terminations was calculated and energy profiles are depicted in Fig. 8. On T_1, T_2, T_3, and T_4 terminations, formation barriers were 7.45 kcal mol^{-1}, 15.08 kcal mol^{-1}, 20.89 kcal mol^{-1}, and 12.15 kcal mol^{-1}, respectively. Based on adsorption energies, which were described in ESI† in the adsorption performance section, desorption barriers of H_2O on T_1 were 25.50 kcal mol^{-1}, 12.57 kcal mol^{-1} for T_2 termination, 21.68 kcal mol^{-1} for T_3 termination, and 14.30 kcal mol^{-1} for T_4 termination.

Table 2 E_{sep} and E_a (both in kcal mol^{-1}) of elementary steps along the most favorable pathway on T_3 and T_4 terminations at 0 K

		T_3				T_4			
		E_{sep}		E_a		E_{sep}		E_a	
	Elementary steps	Calc.	Ref.[a]	Calc.	Ref.[a]	Calc.	Ref.[a]	Calc.	Ref.[a]
1	CO + H → CHO	8.60	8.30	39.73	33.44	1.02	5.30	16.51	18.68
2	CHO + H → CH_2O	−4.61	−11.07	18.06	18.22	−1.49	1.38	17.56	28.37
3	CH_2O + H → CH_2OH	−4.67	−11.99	17.00	20.29	−0.57	−2.31	10.71	14.53
4	CH_2OH → CH_2 + OH	−10.85	−6.69	23.55	21.91	−20.09	−12.91	18.37	21.91
5	CH_2 + H → CH_3	−6.89	−4.61	15.44	22.37	−14.79	−13.14	9.07	18.22
6	CH_3 + H → CH_4	−26.21	−29.06	3.35	12.22	−15.39	−22.60	20.56	25.14

[a] Corresponds to ref. 28, where the calculations were performed with the DMol³ program, DNP, ECP, and PW91, with convergence tolerances of maximum displacement set as 5.0×10^{-3} Å.

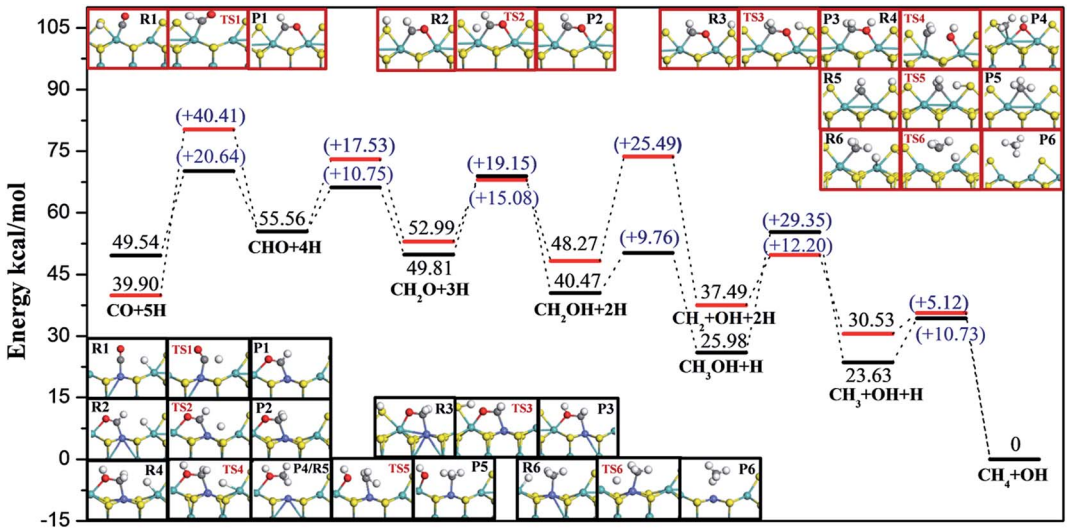

Fig. 6 Energy profiles and configurations along the most favorable CO methanation reaction routes on T_1 and T_3 terminations at 750 K, in which the black lines and structures in black frames represent T_1 termination, while red lines and structures in red frames represent T_3 termination. Zero energy corresponds to the adsorption of the final product CH_4 on T_1 or T_3 terminations.

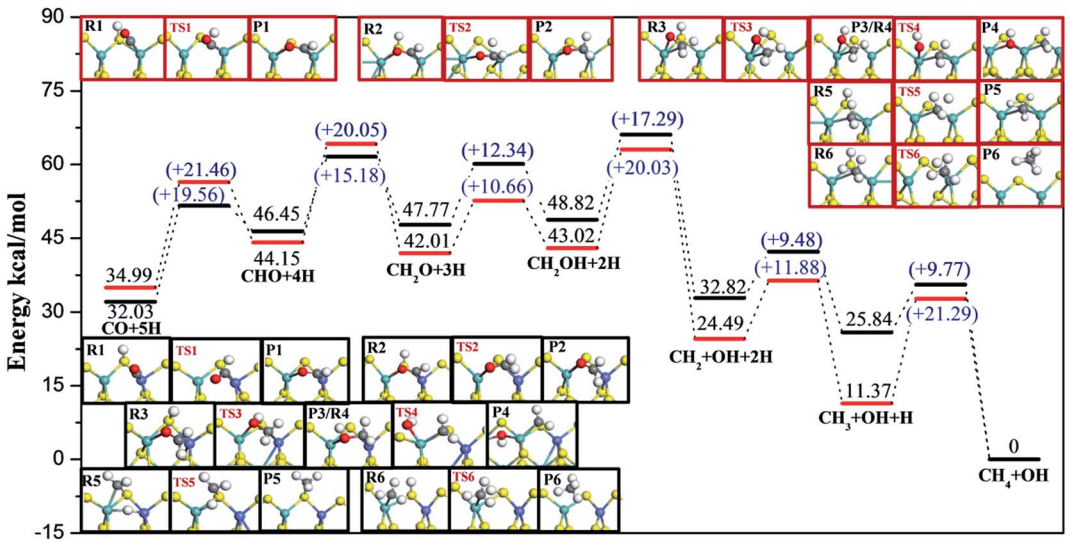

Fig. 7 Energy profiles and configurations along the most favorable CO methanation reaction routes on T_2 and T_4 terminations at 750 K, in which the black lines and structures in black frames represent T_2 termination while red lines and structures in red frames represent T_4 termination. Zero energy corresponds to the adsorption of the final product CH_4 on T_2 or T_4 terminations.

Compared to the reaction of C1 species discussed above, the OH species was not difficult to remove because of relatively low reaction barriers. Moreover, the OH species was found to be more easily removed as H_2O on S terminations for both MoS_2 and for Co–MoS_2 catalysts, and Co-promoter also facilitated the removal of OH species to guarantee enough vacant active sites for C1 hydrogenation on both S termination and Mo termination.

4. BEP relationship

The Brønsted–Evans–Polanyi (BEP) linear relationship[64] between E_{TS} (transition state energy) and E_{FS} (product state energy) of the dissociation of CHO (C–H), CH_2O (C–H), CH_2OH (O–H), CH_3OH (C–O), CH_4 (C–H) on the Mo edge and the dissociation of CHO (C–H), CH_2O (C–H), CH_2OH (O–H), CH_3 (C–H), CH_4 (C–H) on the S edge of the Co–MoS_2 catalyst was investigated, in which dissociation reactions were seen as being in the reverse direction of corresponding formation reactions. The configurations of all reactants, transition states, and products for the above reaction steps can be seen in Fig. 6 and 7, respectively. E_{TS} is calculated from eqn (4), and E_{FS} is calculated from eqn (5), in which $E_{(TS/slab)}$ means the total energy of the transition state with the catalyst slab, $E_{(FS/slab)}$ is the total energy of adsorbed product with catalyst slab, $E_{(slab)}$ is the energy of the clean surface, and $E_{(gas)}$ is the energy of the reactant molecule in the free state.

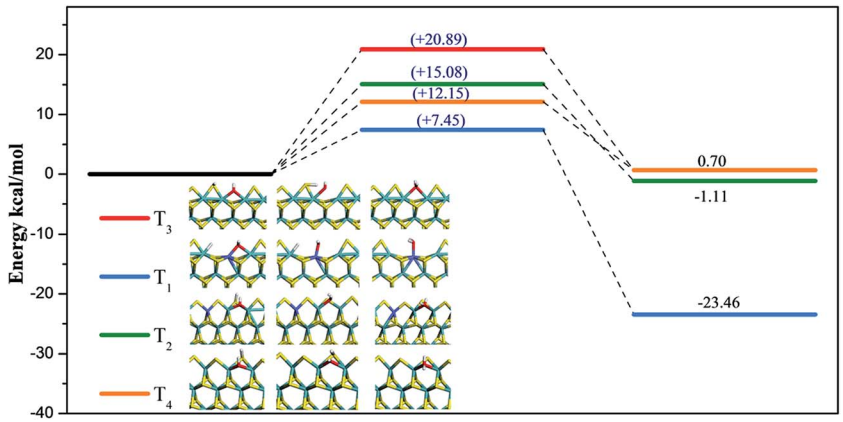

Fig. 8 Energy profiles of H_2O formation by OH reaction with H adatom, in which T_1, T_2, T_3, and T_4 terminations are represented by the blue line, green line, red line, and orange line, respectively. Zero energy corresponds to the co-adsorption of OH species and H adatom.

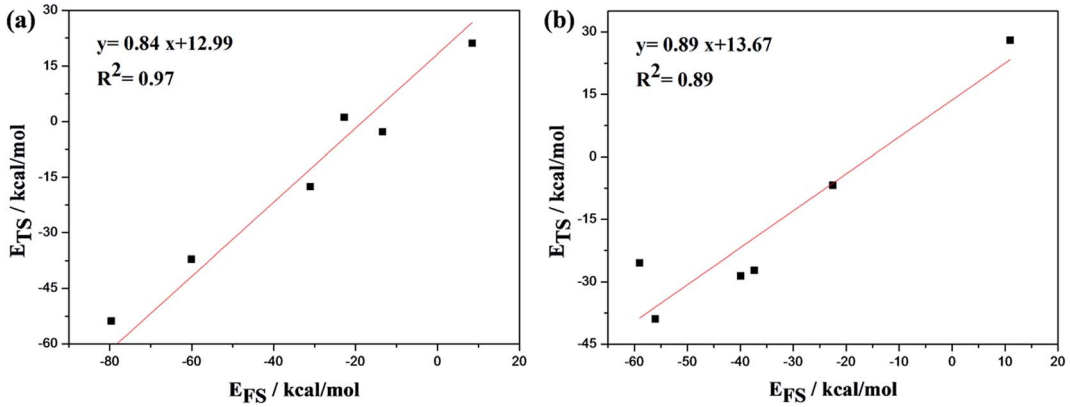

Fig. 9 BEP relationship between the transition-state energy (E_{TS}) and product-state energy (E_{FS}) over Co–MoS_2 catalyst for the CO methanation reaction, in which (a) corresponds to the Mo edge, and (b) to the S edge. The energies of free reactant in the gas and clean catalyst slab (E_{gas} + E_{slab}) were taken as energy references.

$$E_{TS} = E_{(TS/slab)} - E_{(gas)} - E_{(slab)} \quad (4)$$

$$E_{FS} = E_{(FS/slab)} - E_{(gas)} - E_{(slab)} \quad (5)$$

Fig. 9(a) represents the Mo edge of the Co–MoS_2 catalyst, and Fig. 9(b) is the S edge of Co–MoS_2. As seen, the slopes for E_{TS} as a function of E_{FS} are 0.84 for the Mo edge and 0.89 for the S edge, within the range (0 < slope <1) expected. Both slope values were close to 1, indicating the similarity between the configurations of transition states and the corresponding final states, which agreed well with our calculation results, as can be seen in Fig. 6 and 7.

5. Conclusion

The DFT + D method was applied to investigate the CO methanation mechanism on Co–MoS_2 catalysts and to determine the effect of Co. Adsorption calculations indicated that after Co doping, more active sites were created and the Co site and adjoining Mo–Co site were preferable for the adsorption of most C1 intermediates involved. After doping Co-promoter, the reaction mechanism on Mo termination was changed, along which the CH_3OH intermediate was formed by CH_2OH hydrogenation, and it showed that CH_3OH was one kind of side gas product, which accounted for some experimental results in which CH_3OH was detected as a gas product of CO methanation.[56,57] However, the most favorable route on S termination of Co–MoS_2 catalysts stayed the same as that on pure MoS_2; the CH_2OH species was formed in both and then dissociated into CH_2 and OH. The dissociation of CH_3OH was found to be the rate determining step for Mo termination of Co–MoS_2 catalysts at 750 K, and the formation of CHO was the rate-determining step for S termination at 750 K. Furthermore, for pure MoS_2 catalysts, the CO methanation reaction was favored on S termination instead of Mo termination, while after Co-promoter doping, the priority difference between Mo termination and S termination for CO methanation was reduced. Moreover, the reaction enhancement of Co-promoter was more significant on Mo termination than on S termination, since the overall reaction barrier was lowered by 11 kcal mol^{-1} for the Mo edge, and by only 2 kcal mol^{-1} on the S edge. OH species were found to be removed more easily as H_2O after Co-promoter doping on both

the Mo edge and S edge, and the timely removal of OH ensured that active sites were vacant for the adsorption and further reaction of C1 species to produce methane. In addition, the data obtained in this paper were found to agree well with the BEP relationship.

Acknowledgements

The work was supported by the National Natural Science Foundation of China (21336011, 21476260, 21236009, and U1162204) and Science Foundation of China University of Petroleum, Beijing (2462015YQ0311).

References

1 H. Liu, S. Yang, J. Hu, F. Shang, Z. Li, C. Xu, J. Guan and Q. Kan, *Fuel Process. Technol.*, 2012, **96**, 195–202.
2 D. Hu, J. Gao, Y. Ping, L. Jia, P. Gunawan, Z. Zhong, G. Xu, F. Gu and F. Su, *Ind. Eng. Chem. Res.*, 2012, **51**, 4875–4886.
3 J. Kopyscinski, T. J. Schildhauer and S. M. A. Biollaz, *Fuel*, 2010, **89**, 1763–1783.
4 J. K. Nørskov, F. Abild-Pedersen, F. Studt and T. Bligaard, *Proc. Natl. Acad. Sci. U. S. A.*, 2011, **108**, 937–943.
5 A. C. Lausche, A. J. Medford, T. S. Khan, Y. Xu, T. Bligaard, F. Abild-Pedersen, J. K. Nørskov and F. Studt, *J. Catal.*, 2013, **307**, 275–282.
6 J. Yang, Y. Qi, J. Zhu, Y. Zhu, D. Chen and A. Holmen, *J. Catal.*, 2013, **308**, 37–49.
7 J. Oudar, *Catal. Rev.: Sci. Eng.*, 1980, **22**, 171–195.
8 E. J. Erekson and C. H. Bartholomrw, *Appl. Catal.*, 1983, **5**, 323–336.
9 A. J. Frank, H. A. Dick, J. Goral, A. J. Nelson and M. Grätzel, *J. Catal.*, 1990, **126**, 674–676.
10 P. H. Nielsen, K. Pedersen and J. R. Rostrup-Nielsen, *Top. Catal.*, 1995, **2**, 207–221.
11 B. Wang, G. Ding, Y. Shang, J. Lv, H. Wang, E. Wang, Z. Li, X. Ma, S. Qin and Q. Sun, *Appl. Catal., A*, 2012, **431**, 144–150.
12 S. Zaman and K. J. Smith, *Catal. Rev.*, 2012, **54**, 41–132.
13 J. M. Christensen, P. M. Mortensen, R. Trane, P. A. Jensen and A. D. Jensen, *Appl. Catal., A*, 2009, **366**, 29–43.
14 Z. Li, Y. Fu, M. Jiang, T. Hu, T. Liu and Y. Xie, *J. Catal.*, 2001, **199**, 155–161.
15 M. Y. Kim, S. B. Ha, D. J. Koh, C. Byun and E. D. Park, *Catal. Commun.*, 2013, **35**, 68–71.
16 Z. Li, K. Zhang, W. Wang, J. Qu, Y. Tian, B. Wang and X. Ma, *J. Taiwan Inst. Chem. Eng.*, 2016, **68**, 239–245.
17 J. Liu, E. Wang, J. Lv, Z. Li, B. Wang, X. Ma, S. Qin and Q. Sun, *Fuel Process. Technol.*, 2013, **110**, 249–257.
18 C. Lin, H. Wang, Z. Li, B. Wang, X. Ma, S. Qin and Q. Sun, *Front. Chem. Sci. Eng.*, 2013, **7**, 88–94.
19 B. Wang, Y. Yao, M. Jiang, Z. Li, X. Ma, S. Qin and Q. Sun, *J. Energy Chem.*, 2014, **23**, 35–42.
20 H. Wang, C. Lin, Z. Li, B. Wang and X. Ma, *Bull. Korean Chem. Soc.*, 2015, **36**, 74–82.
21 Y. Wang, Y. Su, M. Zhu and L. Kang, *Int. J. Hydrogen Energy*, 2015, **40**, 8864–8876.
22 T. L. Wind, H. Falsig, J. Sehested, P. G. Moses and T. Nguyen, *J. Catal.*, 2016, **342**, 105–116.
23 X. Han, J. Yang, B. Han, W. Sun, C. Zhao, Y. Lu, Z. Li and J. Ren, *Int. J. Hydrogen Energy*, 2016, 1–16.
24 J. Sehested, S. Dahl, J. Jacobsen and J. R. Rostrup-Nielsen, *J. Phys. Chem. B*, 2005, **109**, 2432–2438.
25 S. Fujita, H. Terunuma, M. Nakamura and N. Takezawa, *Ind. Eng. Chem. Res.*, 1991, **30**, 1146–1151.
26 M. Huang and K. Cho, *J. Phys. Chem. C*, 2009, **113**, 5238–5243.
27 N. Koizumi, G. Bian, K. Murai, T. Ozaki and M. Yamada, *J. Mol. Catal. A: Chem.*, 2004, **207**, 173–182.
28 X. Shi, H. Jiao, K. Hermann and J. Wang, *J. Mol. Catal. A: Chem.*, 2009, **312**, 7–17.
29 A. Andersen, S. M. Kathmann, M. A. Lilga, K. O. Albrecht, R. T. Hallen and D. Mei, *Catal. Commun.*, 2014, **52**, 92–97.
30 B. Delley, *J. Chem. Phys.*, 1990, **92**, 508.
31 B. Delley, *J. Chem. Phys.*, 2000, **113**, 7756–7764.
32 B. Delley, *J. Phys. Chem.*, 1996, **100**, 6107–6110.
33 S. Kurth, J. P. Perdew and P. Blaha, *Int. J. Quantum Chem.*, 1999, **75**, 889–909.
34 J. P. Perdew, K. Burke and M. Ernzerhof, *Phys. Rev. Lett.*, 1996, **77**, 3865–3868.
35 S. Grimme, *J. Comput. Chem.*, 2006, **27**, 1787–1799.
36 T. A. Halgren and W. N. Lipscomb, *Chem. Phys. Lett.*, 1977, **49**, 225–232.
37 M. Sun, A. E. Nelson and J. Adjaye, *Catal. Today*, 2005, **105**, 36–43.
38 S. Cristol, J. F. Paul, E. Payen, D. Bougeard, S. Clémendot and F. Hutschka, *J. Phys. Chem. B*, 2000, **104**, 11220–11229.
39 S. Cristol, J. F. Paul, E. Payen, D. Bougeard, S. Clémendot and F. Hutschka, *J. Phys. Chem. B*, 2002, **106**, 5659–5667.
40 P. Raybaud, J. Hafner, G. Kresse, S. Kasztelan and H. Toulhoat, *J. Catal.*, 2000, **189**, 129–146.
41 A. Travert, C. Dujardin, F. Maugé, S. Cristol, J. F. Paul, E. Payen and D. Bougeard, *Catal. Today*, 2001, **70**, 255–269.
42 M. Sun, J. Adjaye and A. E. Nelson, *Appl. Catal., A*, 2004, **263**, 131–143.
43 M. Sun, A. E. Nelson and J. Adjaye, *J. Catal.*, 2004, **226**, 41–53.
44 G. Bian, Y. Fu and M. Yamada, *Appl. Catal., A*, 1996, **144**, 79–91.
45 J. V. Lauritsen, E. Lægsgaard, I. Stensgaard, J. K. Nørskov, B. S. Clausen, H. Topsøe, F. Besenbacher and S. Helveg, *Phys. Rev. Lett.*, 2000, **84**, 951–954.
46 J. V. Lauritsen, M. V. Bollinger, E. Lægsgaard, K. W. Jacobsen, J. K. Nørskov, B. S. Clausen, H. Topsøe and F. Besenbacher, *J. Catal.*, 2004, **221**, 510–522.
47 J. V. Lauritsen, J. Kibsgaard, G. H. Olesen, P. G. Moses, B. Hinnemann, S. Helveg, J. K. Nørskov, B. S. Clausen, H. Topsøe, E. Lægsgaard and F. Besenbacher, *J. Catal.*, 2007, **249**, 220–233.
48 H. Schweiger, P. Raybaud, G. Kresse and H. Toulhoat, *J. Catal.*, 2002, **207**, 76–87.
49 M. Sun, A. E. Nelson and J. Adjaye, *J. Catal.*, 2004, **226**, 32–40.
50 Y. Chen, M. Dong, J. Wang and H. Jiao, *J. Phys. Chem. C*, 2010, **114**, 16669–16676.

51 P. Raybaud, J. Hafner, G. Kresse, S. Kasztelan and H. Toulhoat, *J. Catal.*, 2000, **190**, 128–143.
52 E. Krebs, B. Silvi and P. Raybaud, *Catal. Today*, 2008, **130**, 160–169.
53 L. S. Byskov, B. Hammer, J. K. Nørskov, B. S. Clausen and H. Topsøe, *Catal. Lett.*, 1997, **47**, 177–182.
54 L. S. Byskov, J. K. Nørskov, B. S. Clausen and H. Topsøe, *Catal. Lett.*, 2000, **64**, 95–99.
55 X. Shi, S. Wang, J. Hu, H. Wang, Y. Chen, Z. Qin and J. Wang, *Appl. Catal., A*, 2009, **365**, 62–70.
56 Y. Li, R. Wang and L. Chang, *Catal. Today*, 1999, **51**, 25–38.
57 M. Rothaemel, H. W. Zanthoff and M. Baerns, *Catal. Lett.*, 1994, **28**, 321–328.
58 R. M. Kiai, A. Tavasoli and A. Karimi, *React. Kinet., Mech. Catal.*, 2016, **117**, 173–188.
59 C. R. F. Lund, *Ind. Eng. Chem. Res.*, 1996, **35**, 3067–3073.
60 Y. Lian, H. Wang, W. Fang and Y. Yang, *J. Nat. Gas Chem.*, 2010, **19**, 61–66.
61 Y. Lian, H. Wang, Q. Zheng, W. Fang and Y. Yang, *J. Nat. Gas Chem.*, 2009, **18**, 161–166.
62 A. R. de la Osa, A. De Lucas, A. Romero, P. Casero, J. L. Valverde and P. Sánchez, *Fuel*, 2012, **97**, 428–434.
63 A. R. de la Osa, A. De Lucas, A. Romero, J. L. Valverde and P. Sánchez, *Int. J. Hydrogen Energy*, 2011, **36**, 9673–9684.
64 R. A. V. Santen, M. Neurock and S. G. Shetty, *Chem. Rev.*, 2010, **110**, 2005–2048.